Supporting Information

Hydrogenation of Alkenes, Cycloalkenes, and Arene Side Chains at Lewis Acid-Base Pairs: Kinetics, Elementary Steps, and Thermodynamic Implications for Reverse Reactions

Nicholas R. Jaegers,[1] Mikalai Artsiusheuski, [1] Vardan Danghyan,[1] Junnan Shangguan,[1] Carlos Lizandara-Pueyo,[2] and Enrique Iglesia[1,3*]

[1]Department of Chemical and Biomolecular Engineering, University of California at Berkeley, Berkeley, CA 94720, United States

[2]BASF SE, 67056 Ludwigshafen am Rhein, Germany

[3]Davidson School of Chemical Engineering, Purdue University, West Lafayette, IN 47907, United States

*Email: iglesia@berkeley.edu

S.1 Calculation of enthalpies and entropies using statistical mechanics formalisms

Free energies were computed for a given state as the difference of enthalpy and entropy contributions:

$$G = H - TS \tag{S1}$$

The enthalpy of a given step reflects the sum of contributions from the DFT electronic energy (E_0), the zero-point vibrational enthalpy (E_{ZPV}), and vibrational, translational, and rotational enthalpy (H_{vib}, H_{trans}, and H_{rot}):

$$H = E_0 + E_{ZPV} + H_{vib} + H_{trans} + H_{rot} \tag{S2}$$

DFT-derived vibrational frequencies were used to compute E_{ZPV} and H_{vib}:

$$E_{ZPV} = \sum \frac{1}{2} h\nu_i \tag{S3}$$

$$H_{vib} = \sum \frac{h\nu_i e^{\frac{-h\nu_i}{k_B T}}}{1 - e^{\frac{-h\nu_i}{k_B T}}} \tag{S4}$$

Where h is Planck's constant, ν_i is a vibrational frequency mode, k_B is Boltzmann's constant, and T is temperature. Translational and rotational entropies were computed by:

$$H_{trans} = \frac{1}{2} k_B T \tag{S5}$$

$$H_{rot,linear} = k_B T \text{ or } H_{rot,nonlinear} = \frac{3}{2} k_B T \tag{S6}$$

Entropic contributions can likewise be decomposed into vibrational, translational, and rotational components:

$$S = S_{elec} + S_{vib} + S_{trans} + S_{rot} \tag{S7}$$

Where the contributions are:

$$S_{elec} = Rln[2S + 1] \tag{S8}$$

Where S is the spin multiplicity (0 for singlet, 0.5 for doublet, 1 for triplet, etc.).

$$S_{vib} = \sum_{i=1}^{3N-5} \left[\frac{h\nu_i \, e^{\frac{-h\nu_i}{k_B T}}}{T\left(e^{\frac{-h\nu_i}{k_B T}} - 1 \right)} - k_B ln\left(1 - e^{\frac{-h\nu_i}{k_B T}} \right) \right] \tag{S9}$$

$$S^{\circ}_{trans} = R\left(ln\left[\left(\frac{2\pi M k_B T}{h^2}\right)^{\frac{3}{2}} \cdot \frac{V^{\circ}}{N_A}\right] + \frac{5}{2}\right) \quad \text{(S10)}$$

$$S_{rot,nonlinear} = R\left(ln\left(\frac{\pi^{0.5}}{\sigma}\left(\frac{T^3}{\theta_x\theta_y\theta_z}\right)^{0.5}\right) + 1.5\right) \text{ or}$$

$$S_{rot,linear} = R\left(ln\left(\frac{1}{\sigma}\left(\frac{8T\pi^2 I k_B}{h^2}\right)\right) + 1\right) \quad \text{(S11)}$$

where R is the ideal gas constant, M is the molecular mass of the gaseous molecule, V is the molar volume, and N_A is Avogadro's number. The value σ reports the rotational symmetry numbers for the point group. Values of θ_i were computed using the moments of inertia, I_i, about each axis:

$$\theta_{x,y,z} = \frac{h^2}{8\pi^2 I_{x,y,z} k_B} \quad \text{(S12)}$$

S.2 Comparison of C_3H_6 hydrogenation with reported catalyst based on precious metals

Reported rates on precious and transition metal-based catalysts (per mass of catalyst) are shown in Table 2 for catalysts based on Pd,[49-50] Pt,[51-52] Ni,[53] Ir,[54-55] Rh,[55-57] and Co[58] along with the respective reactions condition. In contrast to heterolytic routes on LAB site pairs which are second-order with respect to reactants and devoid of site coverage, these catalysts, many of which are based on homolytic pathways, show a diverse range of rate expressions. The reaction rate order of H_2 is typically from 0.6 to 1 and that for C_3H_6 from 0 to 1. Reported rate expressions for these precious metal catalysts typically feature denominator terms indicative of active site coverage by hydrocarbon-derived species, but these materials are not unified in rate expression. Due to the diverse, and often unreported, nature of their governing rate expressions, comparison of these reported catalysts on the same basis is challenging without invoking assumptions on the reaction orders or activation energies. To circumvent this, the kinetic trends observed for DME-treated *m*-ZrO_2 are invoked to interpolate/extrapolate to the conditions reported for the transition and precious metal-based catalysts. Comparisons are made on a gravimetric basis, since that is most relevant for practical application. Catalysts selected for Table 2 were determined by comparing gravimetric rates of the literature catalysts to those predicted for *m*-ZrO_2 at the conditions reported in the literature. For example, the ratio literature_rate:predicted_ZrO_2_rate that was highest for each metal type was included in the table.

Citations are consistent with the number of the main text:

49. Brandão, L.; Fritsch, D.; Madeira, L. M.; Mendes, A. M., Kinetics of Propylene Hydrogenation on Nanostructured Palladium Clusters. *Chem Eng J* **2004**, *103*, 89-97.

50. Rogers, G. B.; Lih, M. M.; Hougen, O. A., Catalytic Hydrogenation of Propylene and Isobutylene over Platinum. Effect of Noncompetitive Adsorption. *Aiche J* **1966**, *12*, 369-377.

51. Salnikov, O. G.; Kovtunov, K. V.; Barskiy, D. A.; Bukhtiyarov, V. I.; Kaptein, R.; Koptyug, I. V., Kinetic Study of Propylene Hydrogenation over Pt/Al2o3 by Parahydrogen-Induced Polarization. *Appl Magn Reson* **2013**, *44*, 279-288.

52. Ortiz-Soto, L. B.; Monnier, J. R.; Amiridis, M. D., Structure-Sensitivity of Propylene Hydrogenation over Cluster-Derived Bimetallic Pt-Au Catalysts. *Catal Lett* **2006**, *107*, 13-17.

53. Carturan, G.; Enzo, S.; Ganzerla, R.; Lenarda, M.; Zanoni, R., Role of Solid-State Structure in Propene Hydrogenation with Nickel Catalysts. *Journal of the Chemical Society, Faraday Transactions* **1990**, *86*, 739-746.

54. Argo, A. M.; Odzak, J. F.; Goellner, J. F.; Lai, F. S.; Xiao, F. S.; Gates, B. C., Catalysis by Oxide-Supported Clusters of Iridium and Rhodium: Hydrogenation of Ethene, Propene, and Toluene. *The Journal of Physical Chemistry B* **2006**, *110*, 1775-1786.

55. Weber, W. A.; Zhao, A.; Gates, B. C., Nay Zeolite-Supported Rhodium and Iridium Cluster Catalysts: Characterization by X-Ray Absorption Spectroscopy During Propene Hydrogenation Catalysis. *J Catal* **1999**, *182*, 13-29.

56. Zhao, H.; Hsiao, L.-Y.; Rudawski, N. G.; Song, B.; Kuan, P.-C.; Hullender, L.; Hagelin-Weaver, H., Influence of Tio2 Structure on Metal-Support Interactions in Rh/Tio2 Catalysts Probed by Propylene Hydrogenation and Other Techniques. *Appl Surf Sci* **2024**, *654*, 159389.

57. Pinna, F.; Candilera, C.; Strukul, G.; Bonivento, M.; Graziani, M., Catalytic Hydrogenation of Propene over Polymer Supported Rhodium Complexes. *J Organomet Chem* **1978**, *159*, 91-98.

58. Aaserud, C.; Hilmen, A.-M.; Bergene, E.; Eric, S.; Schanke, D.; Holmen, A., Hydrogenation of Propene on Cobalt Fischer–Tropsch Catalysts. *Catal Lett* **2004**, *94*, 171-176.

Table S1. Reported rates and reaction conditions for C_3H_6 hydrogenation of catalysts described in the literature

Catalyst	T (K)	C_3H_6 (kPa)	H_2 (kPa)	Rate	Units	X	T (g-h/mol)	Mass (g)	Flow Rate (cm^3 min^{-1})	Dispersion	mol site/ kg-cat	Metal/ Catalyst Mass Ratio	Ref. DOI
3.9% Zn/SiO_2	473	0.62	3.4	0.3	h^{-1}						0.6		10.1021/cs401116p
Pd	308	10	90	.0028	mol g^{-1} s^{-1}					0.061	0.0453		10.1016/j.cej.2004.07.008
0.6%Pt/Al_2O_3	274	5	95	33.7	lb-mol lb-cat^{-1} h^{-1}							0.006	10.1002/aic.690120230
0.6%Pt/Al_2O_3	294	5	95	27.6	lb-mol lb-cat^{-1} h^{-1}							0.006	
0.6%Pt/Al_2O_3	307	5	95	58.6	lb-mol lb-cat^{-1} h^{-1}							0.006	
Pt/Al_2O_3	373	101.35	101.35	23.7	s^{-1} (mass Pt_s)						0.045 (Pt^{-1})		10.1007/s00723-012-0400-3
0.72% Pt/TiO_2	313	10	20	35	TOF s^{-1}					0.241	0.009	0.0072	10.1007/s10562-005-9725-y
0.89% Pt-1.68% Au/TiO_2	313	10	20	27	TOF s^{-1}						0.004	0.026	
0.77-1.76% Pt_2Au_4/TiO_2	313	10	20	0.07	TOF s^{-1}						0.01	0.025	
2.14% Pt/SiO_2	313	10	20	12	TOF s^{-1}					0.12	0.01	0.021	
Ni(K)	298	11.1	11.1	12	10^{-2} mol g^{-1} h^{-1}								10.1039/FT9908600739
Ni(K)	313	11.1	11.1	13.5	10^{-2} mol g^{-1} h^{-1}								
Ni(K)	313	11.1	11.1	76.5	10^{-2} mol g^{-1} h^{-1}								
Ni(K)	313	11.1	11.1	275	10^{-2} mol g^{-1} h^{-1}								
Ni(T)	313	11.1	11.1	18.8	10^{-2} mol g^{-1} h^{-1}								
Ni(1)	298	11.1	11.1	1.7	10^{-2} mol g^{-1} h^{-1}								
Ni(1)	313	11.1	11.1	1.7	10^{-2} mol g^{-1} h^{-1}								
Ni(1)	313	11.1	11.1	1.85	10^{-2} mol g^{-1} h^{-1}								
Ni(Li)	298	11.1	11.1	10.6	10^{-2} mol g^{-1} h^{-1}								
Ni(Li)	313	11.1	11.1	11.7	10^{-2} mol g^{-1} h^{-1}								
Ni(Li)	313	11.1	11.1	64.5	10^{-2} mol g^{-1} h^{-1}								
Ni(M)	298	11.1	11.1	11	10^{-2} mol g^{-1} h^{-1}								
Ni(M)	313	11.1	11.1	13	10^{-2} mol g^{-1} h^{-1}								

Ni(M)	313	11.1	11.1	34.8	10^{-2} mol g^{-1} h^{-1}								
Ni(M)	313	11.1	11.1	144	10^{-2} mol g^{-1} h^{-1}								
1% Ir_4/γ-Al_2O_3	273	5.33	13.3	0.059	10^{-2} mol g^{-1} h^{-1}							0.01	10.1021/jp0548523
1% IrAgg/γ-Al_2O_3	273	5.33	13.3	0.107	10^{-2} mol g^{-1} h^{-1}							0.01	
1% Ir_4/MgO	273	5.33	13.3	0.026	10^{-2} mol g^{-1} h^{-1}							0.01	
Rh/TiO_2-ANP	353	2.04	2.04			0.91		0.01	98			0.004	10.1016/j.apsusc.2024.159389
Rh/TiO_2-RNP	363	2.04	2.04			0.7		0.01	98			0.004	
Rh/TiO_2-BNP	363	2.04	2.04			0.72		0.01	98			0.004	
Rh/TiO_2-RNR	373	2.04	2.04			0.6		0.01	98			0.004	
Rh/γ-Al_2O_3	313	2	4			0.98		0.01	100			0.004	
[$Rh_6(CO)_{16}$] /NaY	473	0.9	2.1			0.29		0.1	100			0.06	10.1006/jcat.1998.2306
[$Ir_4(CO)_{12}$] /NaY	673	0.9	2.1			0.19		0.1	100			0.06	
[Rh(NBD) ($PolyPPh_2$)$_2$)$^+$	361	25.67	77			0.05	38.6					0.17	10.1016/S0022-328X(00)80883-9
[Rh(NBD) ($PolyPPh_2$) $_2$}$^+$recycled	361	26	78			0.53	38.6					0.17	
[Rh(NBD) (PolyPPhMentByl) $_2$}$^+$recycled	311	23.3	77			0.32	38.6						
12% Co-0.5%Re/TiO_2	393	25.7	154.3	250	g/gCo_s/h					0.037			10.1023/B:CATL.0000020541.28174.c7
12% Co-0.5%Re/ MSA Al_2O_3	393	25.7	154.3	330	g/gCo_s/h					0.09			
12% Co-0.5%Re/ LSA Al_2O_3	393	25.7	154.3	205	g/gCo_s/h					0.06			
12% Co-0.5%Re/ HSA Al_2O_3	393	25.7	154.3	400	g/gCo_s/h					0.09			
12% Co/ HSA Al_2O_3	393	25.7	154.3	406	g/gCo_s/h					0.07			
12% Co-0.5%Re/ LSA Al_2O_3	393	25.7	154.3	201	g/gCo_s/h					0.06			

S.3 Supporting Experimental Data

C_2H_4 and C_3H_6 hydrogenation rates decreased with time in a manner described by first-order deactivation formalisms; the decay in C_2H_4 hydrogenation rates with time is shown in Figure S1. C_2H_4 hydrogenation rates (after initial DME treatment) decreased from about 200 to about 100 mol kg^{-1} h^{-1} over 1.2 ks when C_2H_4/He and H_2 streams were passed through separate O_2/H_2O scrubbers. A subsequent DME treatment (1.2 ks) fully restored initial C_2H_4 hydrogenation rates (second panel). Rates decreased with time on stream from about 200 to 2 mol kg^{-1} h^{-1} over 0.7 ks, a much more rapid deactivation process caused by inlet streams that were not passed through the scrubbers to test the effectiveness of the traps and the role of O_2/H_2O impurities on deactivation (panel 2). The first-order deactivation rate constant (k_d) for C_2H_4 hydrogenation (derived from the trends in Fig. 3) increased from 0.7 to 6.8 ks^{-1} when inlet streams bypassed O_2/H_2O scrubbers before entering the catalyst bed. This is similar to the deactivation rate constant trends observed using (or bypassing) scrubbers for the comparatively more pure C_3H_8 reactants in dehydrogenation reactions (e.g., 0.11 ks^{-1}vs. 1.2 ks^{-1}). A subsequent DME treatment (at 1.9 ks) again restored initial rates (panel 3), indicating that the same species were responsible for deactivation in each panel, but present in higher concentrations when feed streams were not passed through O_2/H_2O scrubbers. Neither He nor O_2 treatments at 723 K for 3.6 ks restored the initial rates after deactivation, indicating that organic residues are not responsible for the noted deactivation and that DME treatments react with strongly-bound species. These results indicate that titration of the most competent sites by H_2O or CO_2 (either present in inlet streams or formed from O_2 traces in them), instead of reaction-derived organic residues, accounts for the observed decrease in rate during contact with reactants.

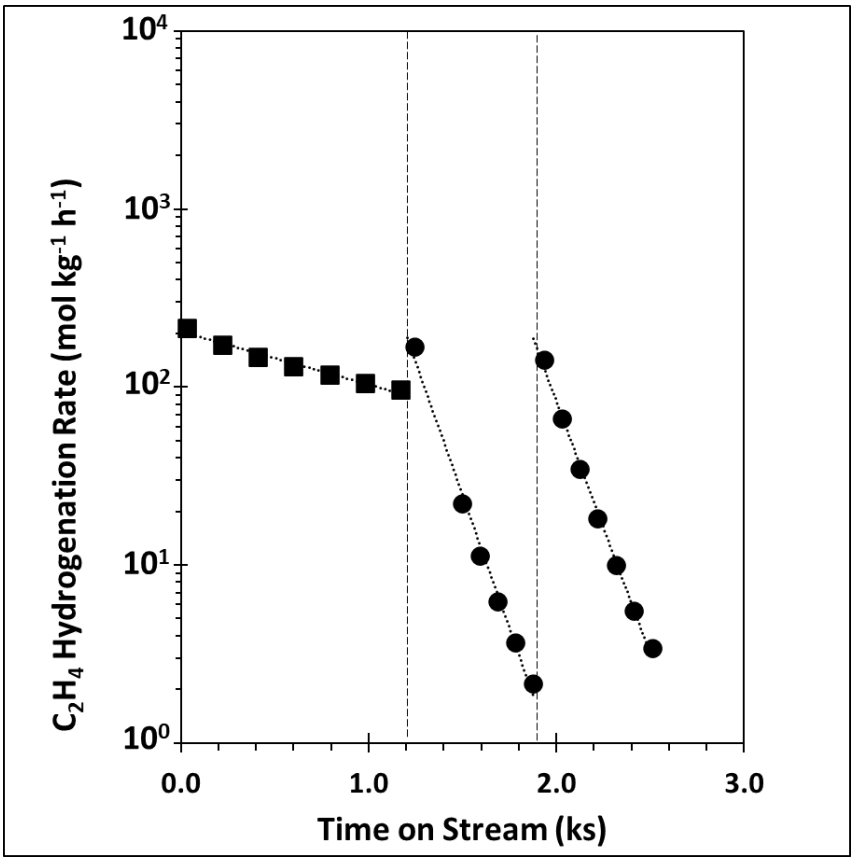

Figure S1. Gravimetric C_2H_4 hydrogenation rate as a function of time on stream (9.2 kPa C_2H_4, 5.6 kPa H_2, 723 K.) after DME treatment at 723 K (0, 1.2 and 1.9 ks, indicated by vertical dashed lines) either after passing C_2H_4/He and H_2 feeds through separate O_2/H_2O scrubbers (squares; panel 1) or by-passing the scrubbers (circles; panels 2 and 3). Dotted lines to guide the eye.

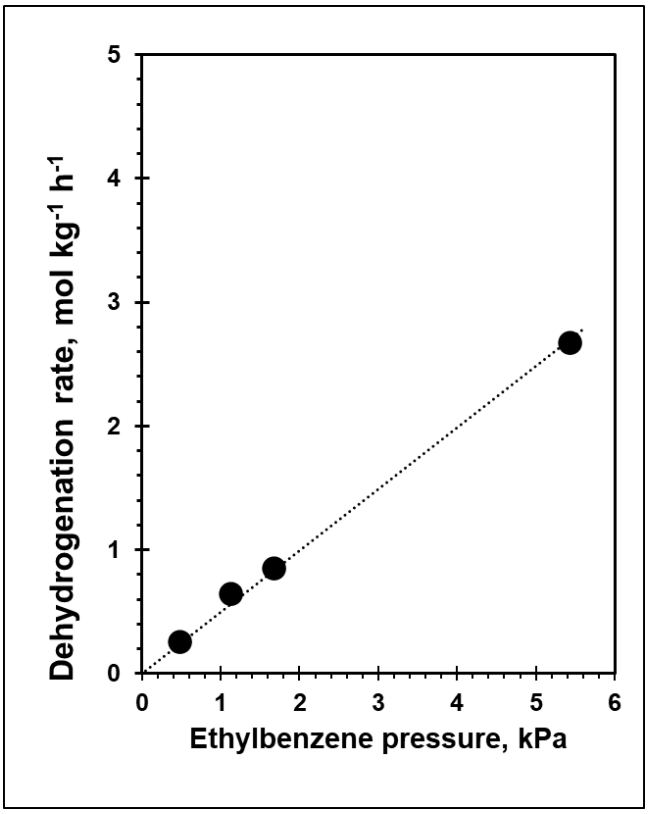

Figure S2. Gravimetric rates of ethylbenzene dehydrogenation on DME-treated *m*-ZrO_2 at 723 K as a function of ethylbenzene pressure (black circles, •••; at 12.5 kPa H_2).

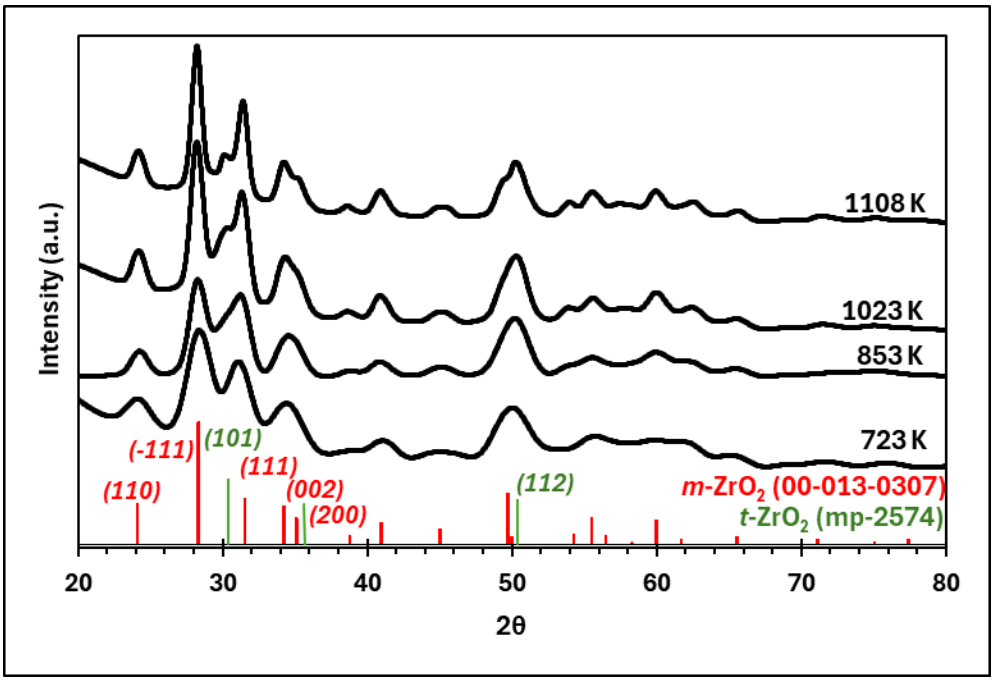

Figure S3. XRD profiles of ZrO_2 after He treatment at 723, 853, 1023, and 1108 K and reference lines for *m*-ZrO_2 (red) and *t*-ZrO_2 (green).

The equilibrium constant for hydrogenation can be expressed as:

$$K_h = e^{-(\Delta G^\circ)/RT} = \frac{kk_BT}{h} e^{-(\Delta S^\circ)/R} e^{-(\Delta H^\circ)/RT} \quad \text{(S13)}$$

Where ΔG°, ΔH°, and ΔS° are the standard Gibbs free energy, enthalpy, and entropy, respectively, and k, k_B, and h are the transmission coefficient, Boltzmann constant, and Planck's constant, respectively. Rate constants for elementary reactions are described by Transition State Theory and are similarly related to activation free energies:

$$k = e^{-(\Delta G^\ddagger)/RT} = \frac{kk_BT}{h} e^{-(\Delta S^\ddagger)/R} e^{-(\Delta H^\ddagger)/RT} \quad \text{(S14)}$$

The measured activation enthalpies for hydrogenation and dehydrogenation are defined relative to the kinetically-relevant TS (which they share) and the respective reference states:

$$\Delta H_h^\ddagger = H^\ddagger - H_{reactants} \quad \text{and} \quad \Delta H_d^\ddagger = H^\ddagger - H_{products} \quad \text{(S15)}$$

Taking the ratio of forward and reverse rate constants (Eq. 5 and combining pre-exponential and entropic terms to A) for hydrogenation and dehydrogenation yields the relations between the heat of reaction and equilibrium constants (Eq. 4). The rate constants for hydrogenation and dehydrogenation are thus linked by thermodynamics:

$$\frac{k_h}{k_d} = \frac{A_h}{A_d} e^{-(\Delta H_h - \Delta H_d)/RT} = K_h \quad \text{(S16)}$$

S.4 Supporting Computational Data

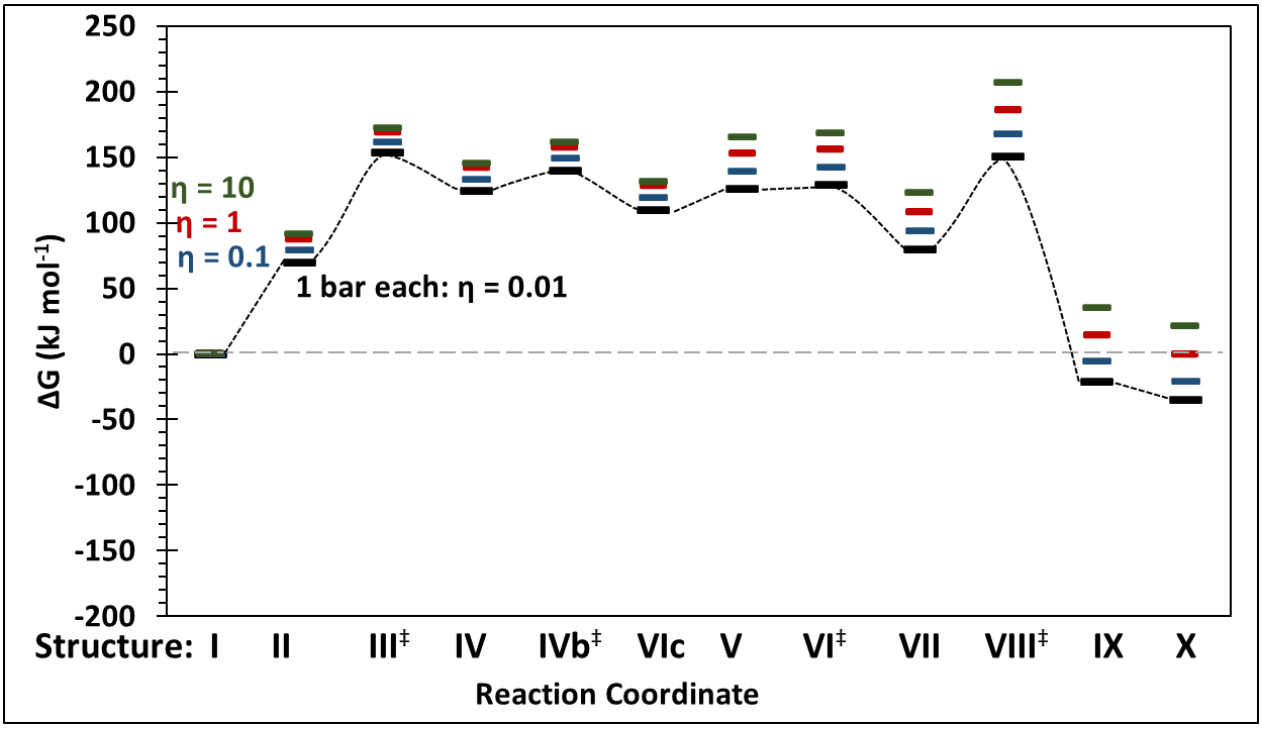

Figure S4. Reaction coordinate diagrams (723 K) for C_3H_6 hydrogenation showing free energies at different approaches to equilibrium (η) of 0.01 (black; the standard reference 1 bar of C_3H_6, H_2, and C_3H_8), and 1 bar total at η=0.1 (blue), η=1 (red), and η=10 (green) with respect to a bare site, $C_3H_{6(g)}$, and $H_{2(g)}$.

Table S2. DFT-derived free energies (ΔG) of C_2H_4 ($_{C2}$) and C_3H_6 ($_{C3}$) hydrogenation on *m*-ZrO_2(-111) at 723 K and 1 bar of reactants and products.

Species	Description	$\Delta G^0{}_{1\ bar}$ (kJ mol^{-1})
I	$ZrO_{2,\ bare}$	0
II	$ZrO_{2,\ H2*}$	+70
III‡	$(ZrO_{2,\ H2*})^{‡}$	154
IV	$ZrO_{2,\ 2H*}$	+124
IVb‡	$(ZrO_{2,\ 2H*})^{‡}$	140
IVc	$ZrO_{2,\ 2H*}$	+110
V_{C2}	$ZrO_{2,\ C2H4\text{-}2H*}$	+142
$VI^{‡}_{C2}$	$(ZrO_{2,\ C2H4\text{-}2H*})^{‡}$	144
VII_{C2}	$ZrO_{2,\ C2H5\text{-}H*}$	+72
$VIII^{‡}_{C2}$	$(ZrO_{2,\ C2H5\text{-}H*})^{‡}$	129
IX_{C2}	$ZrO_{2,\ C2H6*}$	-4
X_{C2}	$ZrO_{2,\ C2H6}$	-55
V_{C3}	$ZrO_{2,\ C3H6\text{-}2H*}$	+126
$VI^{‡}_{C3}$	$(ZrO_{2,\ C3H6\text{-}2H*})^{‡}$	129
VII_{C3}	$ZrO_{2,\ C3H7\text{-}H*}$	+80
$VIII^{‡}_{C3}$	$(ZrO_{2,\ C3H7\text{-}H*})^{‡}$	151
IX_{C3}	$ZrO_{2,\ C3H8*}$	-21
X_{C3}	$ZrO_{2,\ C3H8}$	-35

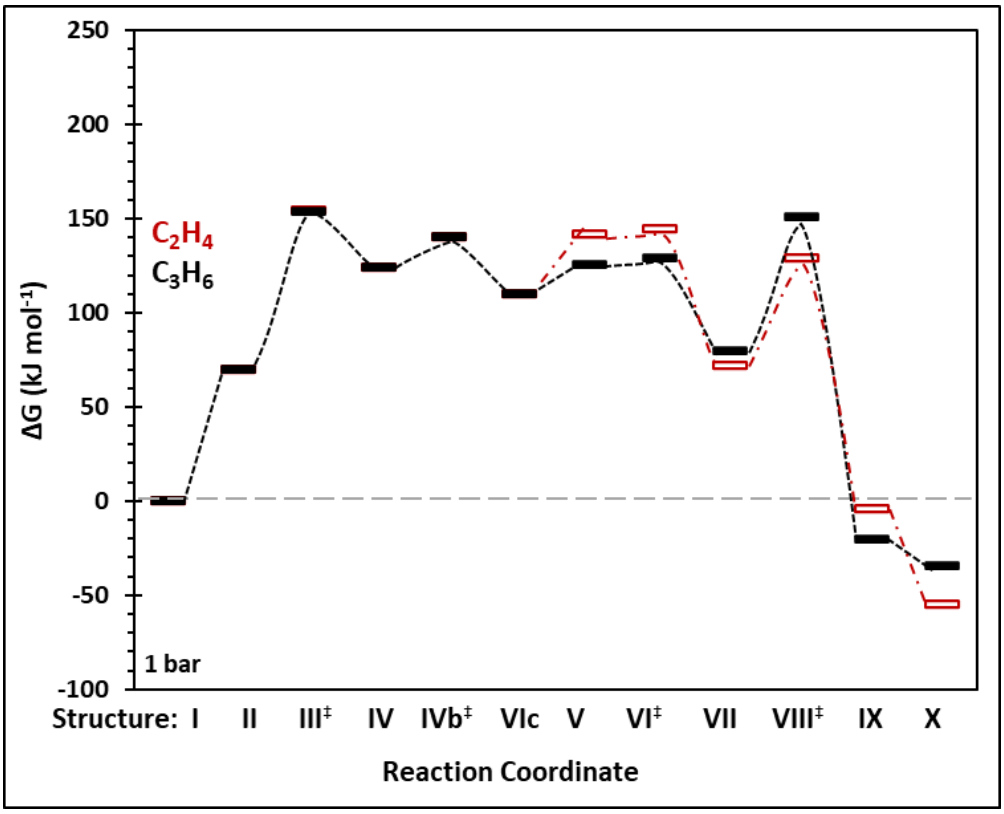

Figure S5. Reaction coordinate diagrams (723 K) for C_2H_4 and C_3H_6 hydrogenation showing free energies at the standard condition of 1 bar for all gas phase species with respect to a bare site, $C_2H_{4(g)}$ or $C_3H_{6(g)}$, and $H_{2(g)}$.